Effect of HCl and HNO_3 on the Synthesis of Pure and Silver-Based WO_3 for Improved Photocatalytic Activity under Sunlight

Priscila Hasse Palharim[1], *Beatriz Lara Diego dos Reis Fusari*[1], *Bruno Ramos*[1], *Larissa Otubo*[2], *Antonio Carlos Silva Costa Teixeira*[1]

(1) Research Group in Advanced Oxidation Processes (AdOx), *Department of Chemical Engineering, Escola Politécnica, University of São Paulo, Av. Prof. Luciano Gualberto, tr. 3, 380, São Paulo, SP, Brazil.*

(2) Instituto de Pesquisas Energéticas e Nucleares (IPEN/CNEN), *Av. Prof. Lineu Prestes, 2242 - Cidade Universitária, São Paulo, SP, Brazil*

ppalharim@usp.br

Abstract

Heterogeneous photocatalysis have been considered an important and efficient alternative water and wastewater treatment process. In this area, different semiconductors, such as tungsten trioxide, have been investigated aiming to enhance photocatalytic performance. WO_3 is known to be an efficient material with high stability in acidic conditions. In the present work, pure and Ag/AgCl-doped WO_3 photocatalysts were synthesized by a simple hydrothermal method. A discussion of the effects of two pH-controlling agents, HCl and HNO_3, in the final properties of the catalyst is reported for the first time. The materials were characterized by XRD, BET, SEM, EDS and UV-vis DRS. All catalysts showed similar or enhanced band gap values compared to a standard photocatalyst benchmark (TiO_2 P25). The type of acid did not lead to significant differences in morphology or photocatalytic activity o undoped catalysts. In contrast, doped catalysts prepared using HCl resulted in particles of flower-like morphology, with higher uniformity and slightly narrower band gap values. Furthermore, the use of HCl in the synthesis of silver-doped WO_3 resulted in catalysts containing AgCl, while Ag^0 was the major dopant species when HNO_3 was used. All materials exhibited good photocatalytic activity, with a maximum of 76.8% acetaminophen degradation under simulated sunlight achieved by the catalyst prepared with HCl and doped with 5% Ag-equivalent. For this catalyst, the degradation kinetics was found to be consistent with the Langmuir-Hinshelwood (L-H) model, and reusability tests showed no significant decrease in the degradation efficiency after four

cycles. Finally, the effects of different scavengers suggest that $O_2^{\bullet-}$ species play a major role in acetaminophen degradation with the containing WO_3, Ag and AgCl.

Keywords

WO_3 photocatalysts, doped WO_3 photocatalysts, simulated sunlight, hydrothermal synthesis, photodegradation.

1. Introduction

Water contamination has become a great challenge due to the discharge of wastewater containing different classes of contaminants of emerging concern which, in some cases, cannot be completely removed by traditional wastewater treatment processes. Therefore, advanced oxidation processes, such as heterogeneous photocatalysis, have been considered important and efficient alternative treatment processes [1,2]. In this context, commercial TiO_2 has been the most widely applied catalyst for this purpose. Despite its low cost, the wide band gap energy (3.0-3.2 eV) and high charge recombination rate are viewed as important drawbacks. In fact, TiO_2 can only harvest UV radiation below 390 nm, which comprises only about 4-5% of the solar spectrum, therefore reducing its application with solar energy [2,3].

Consequently, different semiconductor photocatalysts have been investigated aiming to reduce the band gap energy and enhance light absorption, especially in the visible light region [4]. Tungsten trioxide (WO_3) is a narrow band gap semiconductor with clear response to visible light (2.4-2.8 eV). It is considered an efficient material with high stability in acidic solutions [3,5]. Moreover, WO_3 is generally considered to exhibit photocatalytic activity for both the monoclinic and hexagonal crystalline phases [3]. Nevertheless, the photocatalytic activity of WO_3 is also seriously hindered by the recombination of photogenerated carriers, resulting in reduced process efficiency. This is explained by the WO_3 conduction band edge (about + 0.5 V vs. NHE) being more positive than the oxygen reduction potential ($O_2/O_2^{\bullet-}$ = − 0.33 V vs. NHE), which inhibits the reduction reaction between photogenerated electrons in the conduction band (CB) of WO_3 and adsorbed oxygen molecules [6,7]. Therefore, it is important to modify the photocatalyst to allow the trapping of photogenerated electrons, so that holes in the valence band (VB) are available to oxidize the contaminant molecules rather than being consumed by recombination [6].

In order to overcome this problem, different methodologies have been applied such as morphological modifications [8–10], doping with metals and nonmetals [7,11–13], or combination of WO_3 with other

materials to form heterojunctions [3,14–17]. Silver and silver-based materials are interesting options for doping and for producing heterojunctions with WO_3 catalysts, due to their low cost, low toxicity, high energy absorption in the visible spectrum and ability to enhance photocatalytic activity [3,5]. Some examples of silver-based materials that have been used as photocatalysts are Ag_2S, Ag_2WO_4, Ag_3PO_4, Ag_2MoO_4, Ag_2CO_3, and AgX (X = Cl, Br and I) [18–24]. Among them, AgCl is an attractive material mainly because of its high visible light absorption capacity [25].

Conventionally, crystalline WO_3 can be synthesized through distinct approaches such as the hydrothermal method, sol-gel process, chemical vapor deposition, sputtering and anodization [11,26]. Each synthesis technique can produce materials with certain specific characteristics regarding elemental composition, crystalline structure and surface morphology. The main advantages of the hydrothermal process are the low cost compared with expensive vacuum technologies and the ease of handling [11]. In addition, this method allows for an easy control of morphology, size and crystallinity of the products [26].

The hydrothermal method has been applied to prepare WO_3 catalysts, with reported investigations on the influence of calcination temperature [4,7], presence of surfactants [27] and the influence of oxalic acid and pH in the synthesis [6,9]. Hydrochloric acid is the commonly used acidification agent in the synthesis of WO_3 catalysts with high stability [3,5]. Furthermore, different studies have used the hydrothermal method to synthesize doped WO_3 catalysts varying the dopant concentration and synthesis parameters [3,5,11,29]. Nevertheless, to the best of our knowledge, no systematic study has aimed at evaluating the effects of different acids in the synthesis step of photocatalysts using the one-step hydrothermal method. Also, few studies have estimated the degradation kinetics or the role of different oxidizing species on the degradation of organic contaminants using pure and silver-based WO_3 photocatalysts.

Hence, the current study aims to synthesize pure and doped WO_3 particles through a facile one-step hydrothermal method, evaluating the effect of type of acid (HCl or HNO_3) used during the synthesis procedure at different pH values. The photocatalytic activities of the synthesized materials were evaluated in the heterogeneous photocatalytic degradation of acetaminophen (ACT), selected as a model contaminant. Finally, the degradation kinetics and the role of oxidizing species were investigated.

2. Materials and Methods

2.1. Materials

Sodium tungstate dihydrate ($Na_2WO_4.2H_2O$, ACS, ≥ 99%) and acetaminophen (HPLC, ≥ 99%) were purchased from Sigma-Aldrich. Concentrated hydrochloric acid (36-38% HCl), concentrated nitric acid (65% HNO_3), silver nitrate ($AgNO_3$ ACS, PA) and ethanol were of analytical grade.

2.2. Synthesis of pure and doped WO_3

Pure and doped WO_3 materials were synthesized *via* the one-step hydrothermal method. For synthesizing WO_3, 15 mL of an aqueous solution of 0.3-mol L^{-1} $Na_2WO_4.2H_2O$ was prepared in Milli-Q® water (18.2 MΩ). Then, the pH was adjusted using HCl or HNO_3 to reach pH 0.5, 1.0 or 1.5, producing a total of six materials. Finally, this solution was transferred to a 220-mL PTFE-lined autoclave, which was kept in an oven at 120 °C for 24 h. The solid obtained was subsequently washed by resuspending and centrifuging for three times with ethanol and once with water to remove any possible ionic remnants. The final solution was dried in an oven at 80 °C for 24 h. Ag-doped WO_3 photocatalysts were synthesized by adding $AgNO_3$ to the 0.3 mol L^{-1} $Na_2WO_4.2H_2O$ aqueous solution to achieve WO_3-3% and 5% Ag (w/w). These solutions were kept under magnetic stirring for 1 h, at room temperature. Subsequently, the pH was adjusted to 1.5 using HCl or HNO_3, resulting in four photocatalytic materials. Lastly, the materials were washed and dried as previously described. In addition, the WO_3-5% Ag catalyst synthetized using HCl at pH 1.5 – thereinafter named WO_3-5% (HCl 1.5) – was calcined at 400 °C for 2 h to compare with the non-calcined catalyst.

2.3. Photocatalyst characterization

The morphology of the synthesized materials was investigated by scanning electron microscopy (SEM) and transmission electron microscopy (TEM). For the SEM analyses, a suspension of the sample in isopropanol was dripped on a silicon substrate and dried. Some observations were carried out in a SEM (Vega 3 LMU Tescan equipment), at 5 and 20 kV, and others in a FEG-SEM (JSM-6701F, Jeol) operating at 3 kV. For the TEM analyses, the suspension was dripped on a carbon coated copper grid and a JEM-2100 (Jeol) microscope was used, operating at 200 kV. The chemical composition was analyzed by energy dispersive X-ray spectroscopy (EDS) (Oxford equipment coupled to SEM). X-ray powder diffraction (XRD) patterns were obtained using a D8 Focus Bruker AXS equipment, at 20 kV and 40 mA with a Cu K-α radiation source and Ni filter. Ultraviolet-visible diffuse reflectance spectra (UV-vis DRS) were

recorded on a spectrophotometer Shimadzu 2550, equipped with an integrating sphere. BET surface areas were measured by N_2 adsorption using a Gemini III 2375 equipment (Micromeritics Instrument Corp.).

2.4. Photocatalytic activity assays

Acetaminophen (ACT) was selected as a model contaminant to evaluate the photocatalytic activity of the synthesized materials. In a typical run, the catalyst (10 mg) was dispersed into 10 mL of 5-mg L^{-1} ACT solution, in a 25-mL beaker. The reaction temperature was kept at 21 °C by using a thermal bath. First, the suspension was stirred in the dark for 90 min to achieve adsorption-desorption equilibrium. Then, photocatalytic experiments were conducted under simulated sunlight for 120 min, using a solar simulator (Peccell Inc., PEC-L01), with the light focus placed at 13 cm from the solution surface (Figure S1). The irradiance was 3.4 mW cm^{-2}, measured by a spectroradiometer (Luzchem, SPR-4002). 200-µL samples were collected over time, diluted five times, filtered and analyzed by HPLC. A HPLC Shimadzu LC20 chromatograph with a UV-vis detector (SPD20A), equipped with a C18 column (Prominent), was used to quantify ACT concentration. The mobile phase consisted of methanol:water (25:75), at a flow rate of 1.0 mL min^{-1}; the injection volume and the temperature were 50 µL and 28 °C, respectively. The detection wavelength was 243 nm and the retention time was approximately 7 min. Under these conditions, the limits of ACT detection and quantification were 0.08 mg L^{-1} and 0.24 mg L^{-1}, respectively.

3. Results and Discussion

3.1. Phase structure of the synthesized materials

Figures 1a and 1b show the XRD patterns with indexed peaks of the pure WO_3 catalysts synthesized at pH 0.5, 1.0 and 1.5, using HCl and HNO_3. Samples synthesized at pH 1.0 and 1.5 using HCl or HNO_3 exhibited high crystallinity, with well-defined diffraction peaks. The XRD patterns were found to be a good match for the JCPDS Card No. 96-100-4058 of the W_3O_9 hexagonal structure. Conversely, WO_3 (HCl 0.5) particles seem to present more than one crystal structure. Likewise, in the case of WO_3 (HNO_3 0.5), the XRD pattern indicates the existence of diffraction peaks corresponding to the tungsten oxide anorthic phase (JCPDS Card No. 32-1395). Moreover, all XRD patterns showed to also match the JCPDS Card No. 00-017-0616 of sodium tungsten oxide hydrate.

Figure 1c presents the XRD patterns of the doped WO_3 particles, synthesized using HCl or HNO_3 at pH 1.5. Again, the XRD patterns match the JCPDS Card No. 96-100-4058 of the W_3O_9 hexagonal structure

well. The addition of $AgNO_3$ in the synthesis step resulted in different doped materials, depending on the acid used. For doped catalysts synthesized with HNO_3, although it is hard to identify extra peaks compared to the pure sample, the patterns were found to match the JCPDS Card No. 00-004-0783 of cubic metallic silver crystals [29]. However, HCl when used reacted with $AgNO_3$ producing AgCl, whose diffraction peaks can be indexed to the cubic phase of AgCl (JCPDS Card No. 96-901-1667) [3]. The most evident peaks appeared at 2θ of 27.8°, 32.24°, 46.23° and 54.83°, which are assigned to the crystallographic planes (111), (200), (220) and (311) of cubic AgCl. Hence, it is clear that the synthesized catalysts are composed of Ag, AgCl and WO_3 particles. Also, it is evident that the intensity of diffraction peaks increases by increasing $AgNO_3$ loading [11]. It is worth mentioning that WO_3 is usually considered to show photocatalytic activity for hexagonal and monoclinic phases [3].

Crystallite sizes, calculated by the Scherrer equation (Table 1), did not show any clear trend with the type of acid used or dopant. The effect of crystallite size on photocatalytic performance is still questionable as the improvement in catalytic activity has been found to be related to the increase or decrease in crystallite size by different researchers [30]. Nandiyanto et al. [30] attribute the difficulty in understanding the correlation between crystallite size and activity to the different parameters that govern the photocatalytic process.

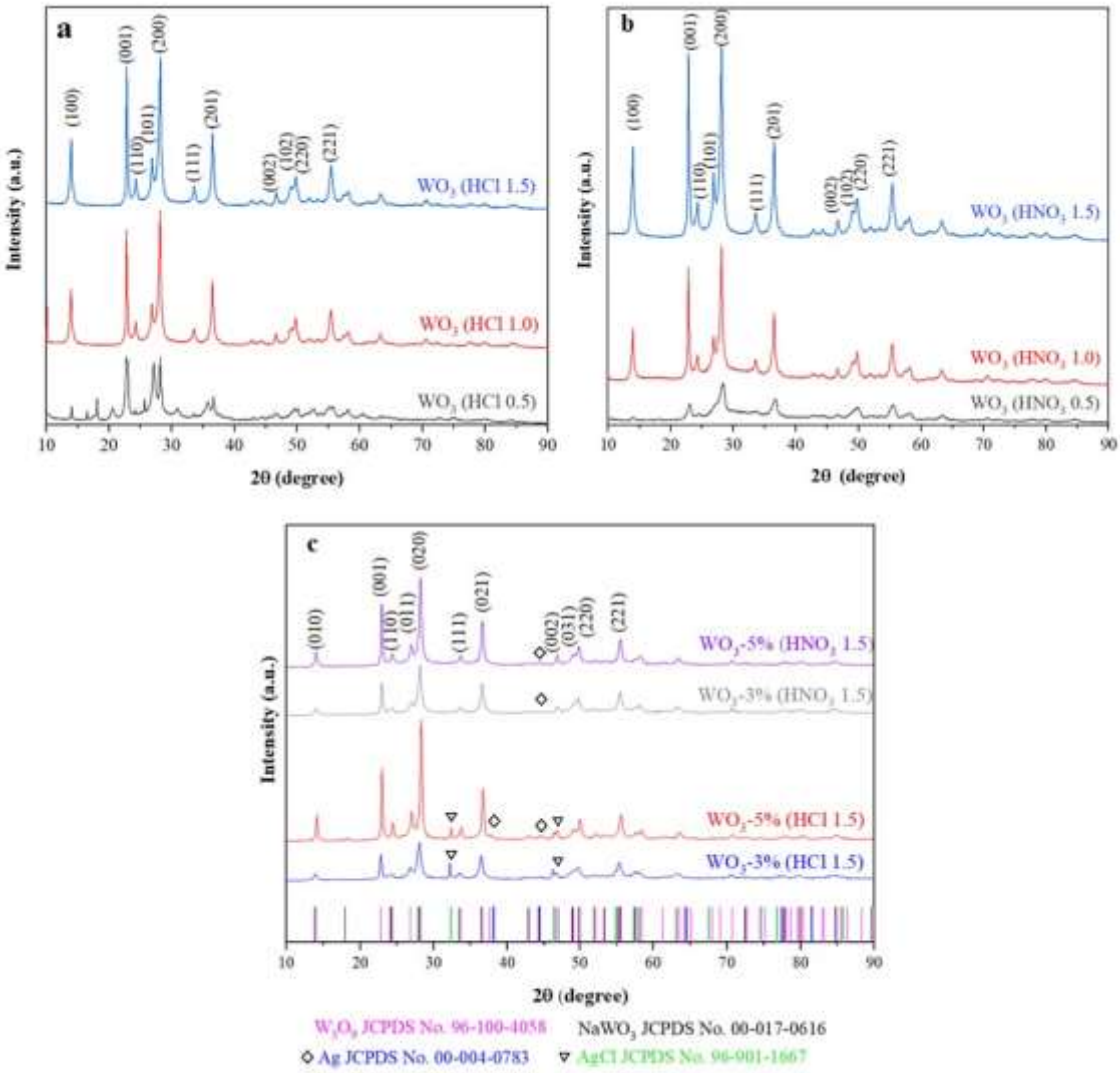

Fig. 1. XRD patterns of pure WO_3 catalysts synthesized by the hydrothermal method using a) HCl at pH 0.5, 1.0, 1.5; b) HNO_3 at pH 0.5, 1.0 and 1.5; and c) doped WO_3 synthesized by the hydrothermal method using 3% and 5% of Ag with HCl or HNO_3 at pH 1.5.

Catalyst	Crystallite size (nm)	Particle size (μm)	Surface area ($m^2 g^{-1}$)	E_g (eV)	λ_g (nm)
WO_3 (HCl 0.5)	29.7	6.6 ± 3.6	51.69	2.98	416
WO_3 (HCl 1.0)	31.0	5.6 ± 3.7	66.37	2.86	433
WO_3 (HCl 1.5)	27.0	4.4 ± 2.6	34.28	2.64	469
WO_3 (HNO_3 0.5)	9.9	5.5 ± 3.0	48.25	3.29	377
WO_3 (HNO_3 1.0)	27.3	6.6 ± 2.2	60.12	3.32	373
WO_3 (HNO_3 1.5)	24.9	5.6 ± 2.2	36.57	3.08	403
WO_3-3% (HCl 1.5)	29.5	4.5 ± 1.8	23.68	2.91	426
WO_3-3% (HNO_3 1.5)	22.3	3.6 ± 1.8	37.59	2.79	444
WO_3-5% (HCl 1.5)	19.8	4.0 ± 0.9	38.61	2.63	471
WO_3-5% (HNO_3 1.5)	27.2	4.6 ± 1.6	23.69	2.64	470
WO_3-5% (HCl 1.5) - calcined	n.d.	n.d.	2.54	2.38	521

The % refers to the nominal silver content (m/m) of the catalyst.

Table 1. N_2-BET surface areas, crystallite size, SEM particle size, band gap energies and absorption edges of pure and doped WO_3 catalysts.

3.2. Morphological structure

Figure 2 and Table 1 show the SEM images and the mean particle sizes, respectively, of the pure and doped WO_3 catalysts. Figures 2a-f reveal that bare WO_3 particles are irregularly shaped with mean particle sizes varying from 4.4 to 6.6 μm. In general, Ag-doping promoted a slightly decrease in particle sizes (Table 1). In contrast, the surface morphology of doped catalysts (Figures 2g-k) is clearly more uniform compared to pure WO_3 catalysts, especially for those with 5% content of dopant. The variation in morphology reveals that the presence of Ag, especially as AgCl, influences WO_3 crystal growth [3].

Flower-like WO_3 particles can be observed in doped WO_3 samples, with mean particle sizes varying from 3.6 to 4.6 μm (Table 1). Despite having the same structural shape, the doped catalysts synthetized using HNO_3 (Figures 2j-k) presented less uniform WO_3 morphology, suggesting that HNO_3 does not facilitate well-organized particle agglomeration. In turn, the doped WO_3 catalysts synthetized using HCl, particularly WO_3-5% (HCl 1.5) (Figures 2h-i) showed a highly uniform flower-like morphology; closer inspection shows that these flower-like structures are nanorod assemblies (Figure 2i).

187 Similar structures are reported by Fang et al. [27], who synthesized WO_3 particles *via* the one-step
188 hydrothermal method using HCl as acidification agent. The authors suggest that the better uniformity of
189 the flower-like structures can be obtained with hydrothermal reaction times higher than 20 h, since the
190 three-dimensional WO_3 nanostructures would grow gradually, resulting in flower-like structures.
191 Therefore, the 24-h hydrothermal synthesis used in our study was clearly sufficient to promote the
192 formation of flower-like structures. This structure formed by several nanorods can positively influence the
193 photodegradation performance, when compared to compact spherical structures, for example. The slow
194 photon effect may be a characteristic of this structure, which can improve the use of light [31].
195
196

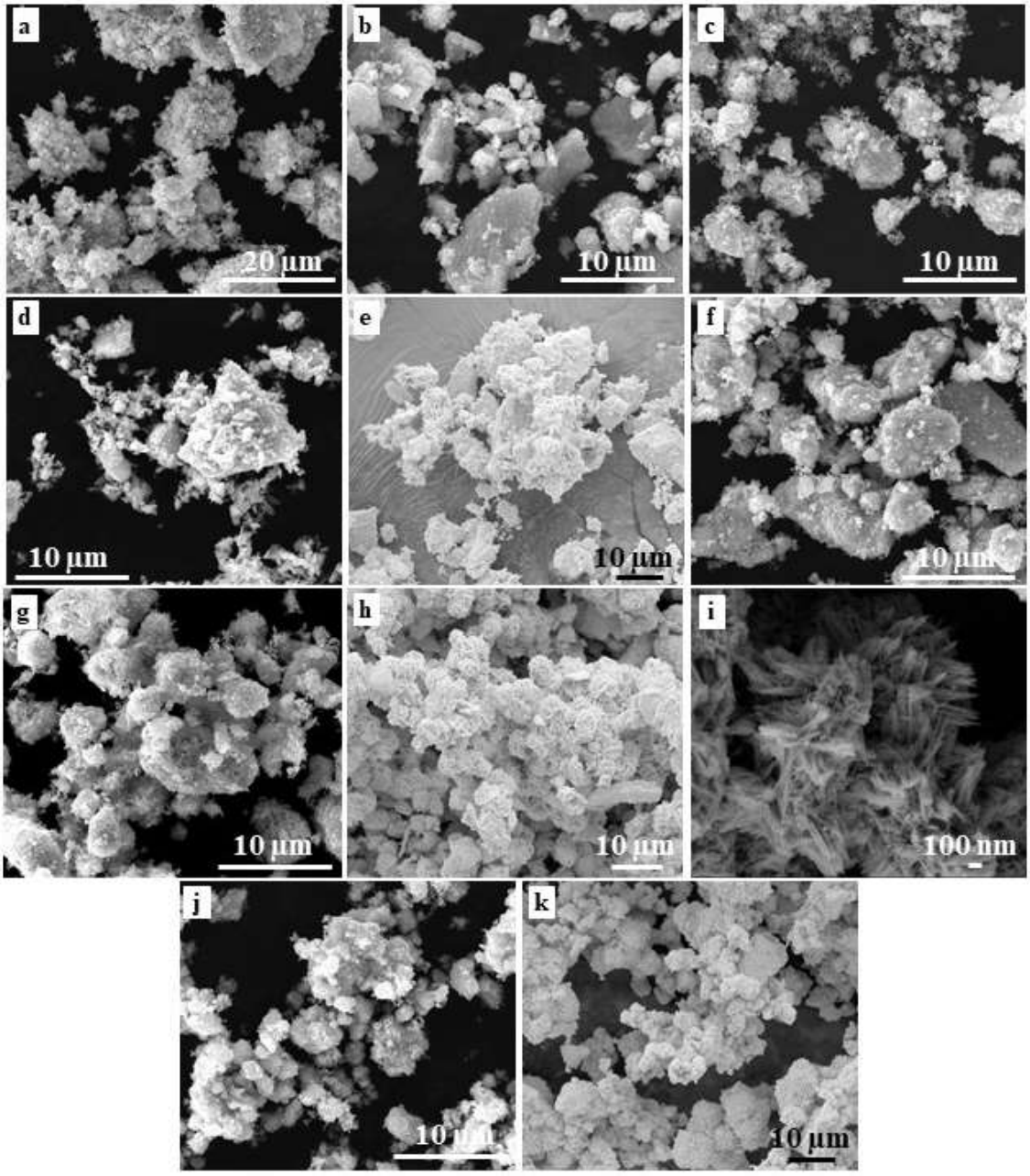

Fig. 2. SEM images of pure WO_3 photocatalysts synthetized using HCl at pH a) 0.5, b) 1.0 and c) 1.5; pure WO_3 photocatalysts synthetized using HNO_3 at pH d) 0.5, e) 1.0 and f) 1.5; doped WO_3 photocatalysts synthetized using HCl at pH 1.5 with g) 3% dopant and h-i) 5% dopant; doped WO_3 photocatalysts synthetized using HNO_3 at pH 1.5 with j) 3% dopant and k) 5% dopant.

A comparative assessment of the elemental mapping and the average chemical composition of the catalyst synthesized with 5% Ag was carried out by energy dispersive spectrometry (EDS). Both the elemental mapping and the EDS spectra, depicted in Figure 3, confirm the presence of W and Ag on doped samples; similarly, Cl was found in the sample synthesized with HCl. No impurity peaks were observed.

Interestingly, the WO_3-5% (HNO_3 1.5) catalyst has a highly uniform distribution of elements (Figure 3b), suggesting that the WO_3 particles are consistently doped with silver. In contrast, the WO_3-5% (HCl 1.5) catalyst presents Ag and Cl at specific sites (Figure 3a), proving the formation of AgCl, as indicated by XRD analysis (Figure 1c). In the scanned region, the WO_3-5% (HCl 1.5) catalyst revealed 63.2% W, 14.1% Ag and 5.8% Cl; while the WO_3-5% (HNO_3 1.5) catalyst showed 84.6% W and 15.4% Ag (atomic percentage).

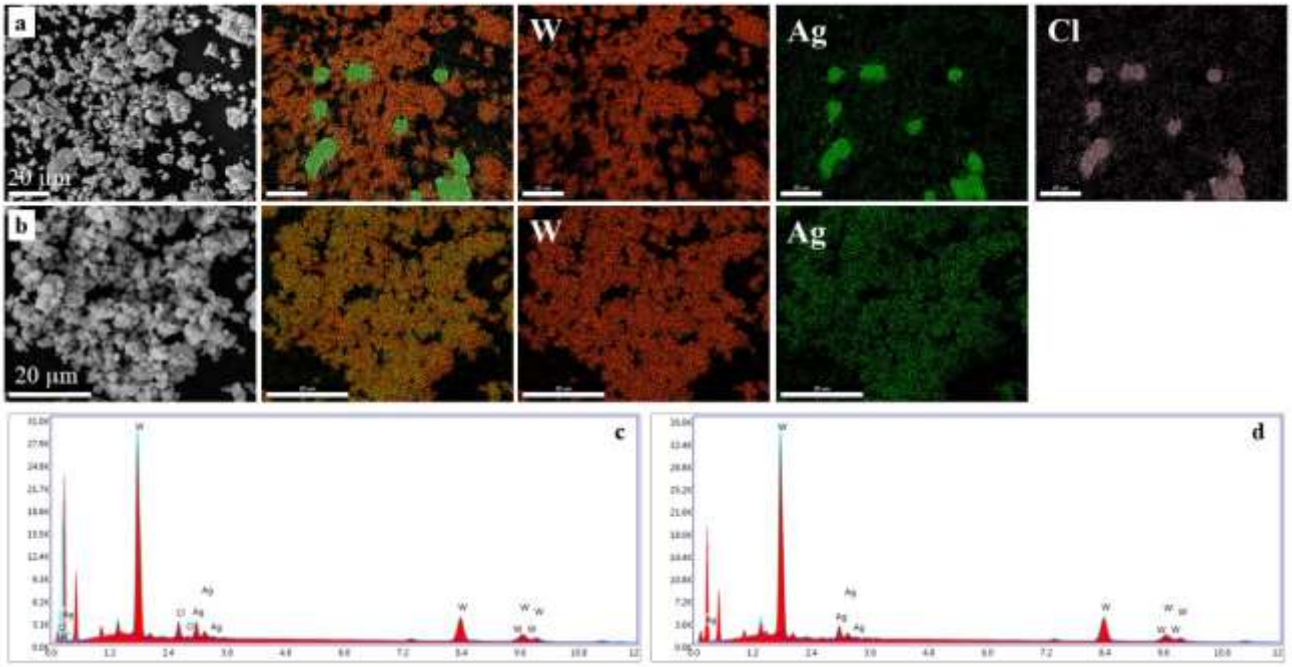

Fig. 3. Energy dispersive spectroscopy elemental mapping images and energy dispersive X-ray spectra (EDS) of a) and c) WO_3-5% (HCl 1.5) catalysts; b) and d) WO_3-5% (HNO_3 1.5) catalysts.

The morphology of WO_3-5% (HCl 1.5) catalyst was analyzed in detail by SEM-FEG. Figure 4 shows the occurrence of smooth spherical-shaped particles with diameters ranging from 1 to 5 µm, which were confirmed as AgCl particles by EDS analyses. This suggests that the WO_3-5% (HCl 1.5) catalyst is not completely uniform; instead, it is made of flower-like WO_3 and smooth spherical-shaped AgCl particles. Interestingly, it can be seen that AgCl particles are covered and/or in contact with WO_3 particles, forming a composite. Although this pattern is not commonly reported for the synthesis of WO_3-AgCl, Chai et al. [32] successfully synthesized similar catalysts through the hydrothermal/photoreduction method, designating them as Ag–AgCl particles decorated with WO_3.

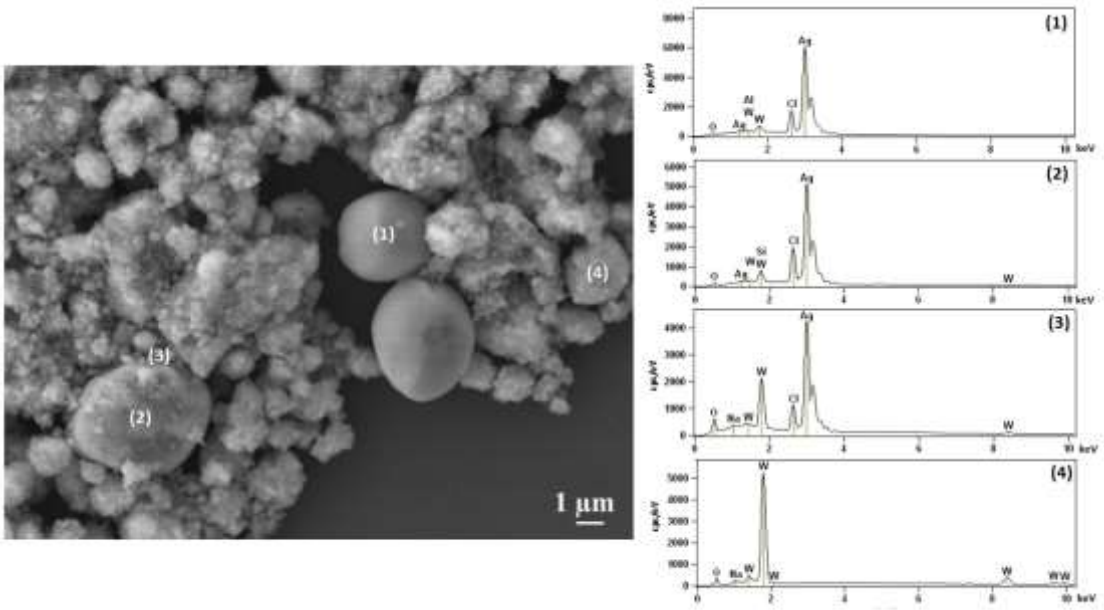

Fig. 4. SEM-FEG image of WO_3-5% (HCl 1.5) catalyst and corresponding energy dispersive X-ray spectra (EDS) at different sites.

In addition, WO_3-5% (HCl 1.5) catalyst was also analyzed by TEM. Figure 5a confirms that WO_3 particles are made of nanorods with length of 20 to 80 nm. It is possible to observe some small, spherical particles adhered to the WO_3 nanorods, which are confirmed to be metallic Ag, with particle diameters ranging from 9 to 37 nm. To better elucidate the presence of WO_3 and Ag, some selected areas were analyzed using high resolution TEM (Figures 5b-c). The high crystallinity of the WO_3 nanorods is demonstrated by the clear lattice boundary in the HRTEM image (Figure 5b). Two lattice spacings were found for the WO_3 phase, 3.65 Å and 6.25 Å, corresponding to the (001) and (010) crystalline planes of hexagonal W_3O_9 (JCPDS Card No. 96-100-4058), corroborating the result obtained by XRD analysis. For the Ag phase (Figure 5c), a lattice spacing of 2.36 Å was detected, which corresponds to the (111) crystalline plane of cubic metallic silver crystals (JCPDS Card No. 00-004-0783). Due to the large size of AgCl particles, their detection by HRTEM was not possible; even so, their presence was proved by SEM-FEG-EDS (Figure 4). In conclusion, the SEM-FEG-EDS and TEM/HRTEM results indicate that the WO_3-5% (HCl 1.5) photocatalyst is a composite consisting of Ag@WO_3@AgCl, suggesting the formation of a complex heterojunction between these three materials.

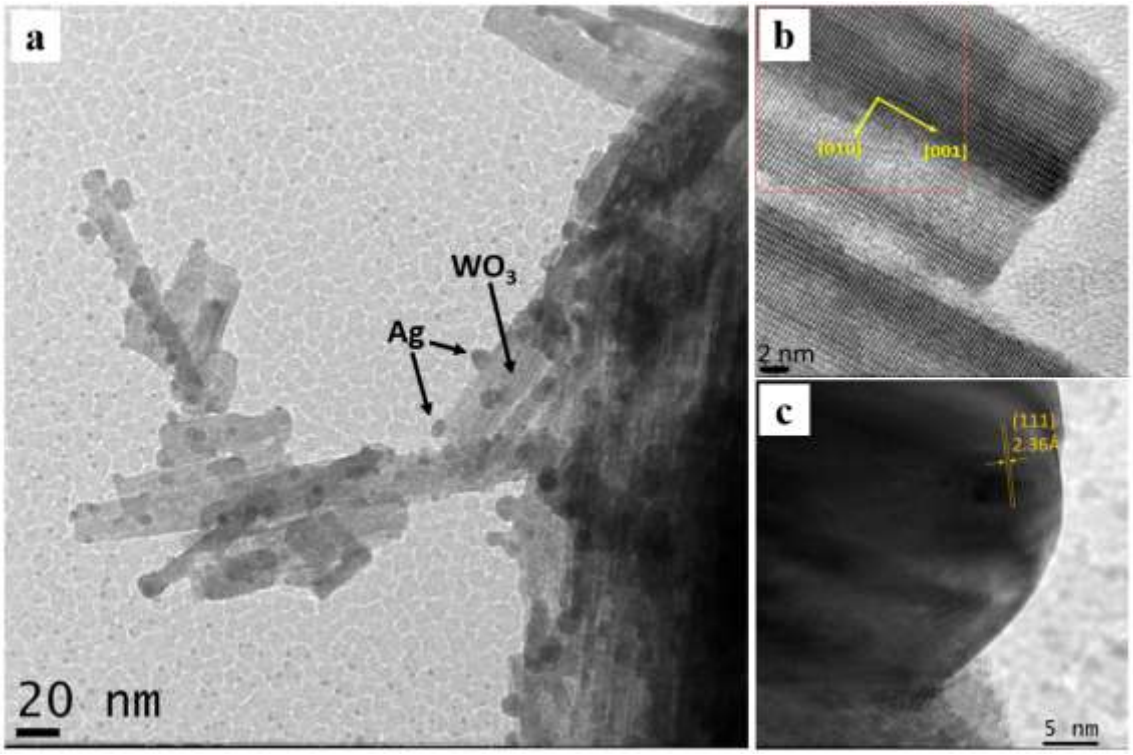

Fig. 5. (a) TEM and HRTEM images of WO_3-5% (HCl 1.5) catalyst showing crystal planes of (b) WO_3 and (c) Ag.

3.3. BET surface areas

Table 1 presents the N_2-BET specific surface areas of pure and doped WO_3 samples. Bare WO_3 catalysts have relatively large surface areas, with higher values shown for catalysts synthetized using HCl or HNO_3 at pH 1.0. The introduction of Ag into WO_3 promoted a slightly decrease in surface areas, which may be associated with increased particle agglomeration following silver incorporation. Pore blockage may also occur, causing a reduction in the surface area [33]. This result is consistent with the work of Yu et al. [3], which reported surface areas of 21 $m^2\ g^{-1}$ and 5 $m^2\ g^{-1}$ for samples of calcined WO_3 particles loaded with 0.25% and 1.25% AgCl, respectively.

For the catalysts synthesized using HNO_3, increasing the Ag content resulted in lower surface areas, due to particle agglomeration. Conversely, for samples synthesized using HCl, an increase in the silver content led to an increase in the surface area. The complex Ag@WO_3@AgCl structure may have contributed to the increase in surface area as more AgCl particles are available.

Note that the relatively high surface areas achieved are coherent with non-calcined WO_3 samples [10]. Hence, the WO_3-5% (HCl 1.5) catalyst was calcined to compare with the non-calcined sample. From Table 1, it is clear that the calcination step drastically reduced the catalyst surface area. The higher calcination

temperature promoted sintering of the particles, which could lead to pore collapse and/or blockage of smaller pores, thereby reducing the surface area and the pore volume as the pore diameter increased [34].

3.4. Optical properties

The UV-vis diffuse reflectance spectra of pure and doped WO_3 photocatalysts synthesized using HCl or HNO_3 at different pH values are displayed in Figure 6. All the catalysts showed strong absorption in the UV region and considerable absorption of visible light, confirming their broad-spectrum activity. According to Yu et al. [10], the intrinsic band gap absorption of tungsten trioxide due to the electron transitions from the valence band to the conduction band ($O_{2p} \rightarrow W_{5d}$) may have resulted in these absorption wavelengths. The coupling of Ag into WO_3 slightly shifts the absorption edge to the visible light region.

The band gap energy was estimated by converting the diffuse reflectance spectra to the Kubelka-Munk function, and then extrapolating the linear slope of the curve to zero reflectance in the Tauc plot (Figure S2). Table 1 shows that the E_g of all the samples was similar or enhanced when compared to commercial TiO_2 (3.0-3.2 eV) [3,5], suggesting that the photocatalytic activity of the synthesized WO_3 materials may be intensified under solar light. In general, there is no significant difference in the E_g values for the catalysts synthesized using HCl or HNO_3, yet those synthesized with HNO_3 have slightly higher values. In contrast, the doped catalysts exhibited lower E_g values compared to the pure materials; also, the E_g values decreased with the increase of the silver content. The WO_3-5% (HCl 1.5) catalyst was calcined to compare with the non-calcined sample. From Table 1, it can be seen that the calcination process resulted in a narrower band gap value and increased absorption in the visible range. Despite this being an advantage for photocatalysis, the surface area was found to be too low (2.54 $m^2\ g^{-1}$), which may reduce the photocatalyst activity.

The increase in the absorption edge observed for doped materials may be due to the localized surface plasmon resonance (LSPR) effect, as it allows the Ag nanoparticles to absorb light in the visible spectrum [35]. When LSPR occurs on the surface of the Ag nanoparticles excited by light, the radiated light is scattered and further absorbed on the Ag surface; as a result, an evanescent wave is generated with a strong electromagnetic field. This evanescent wave is localized on the Ag nanoparticle surface, rather than being propagated, and is kept at a distance from the surface less than the particle diameter. It is well known that LSPR contributes to the improvement of optical phenomena, such as light absorption and Raman scattering [36].

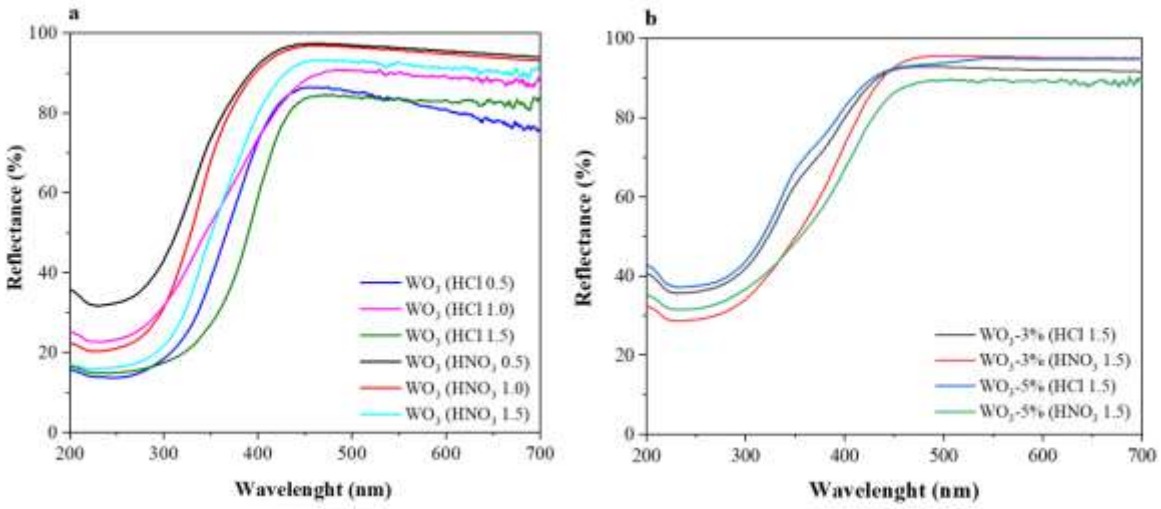

Fig. 6. UV-vis diffuse reflectance spectra of a) pure WO_3 catalysts and b) doped WO_3 catalysts synthesized using HCl or HNO_3.

3.5. Photocatalytic activity

The photocatalytic performances of the pure and doped WO_3 catalysts synthesized using HCl or HNO_3 were evaluated by tracking the degradation of acetaminophen (ACT) under simulated sunlight. No appreciable ACT removal was observed during the first 90-min run under dark conditions. It can be seen from Figure 7 that the pure WO_3 photocatalysts showed poor activity upon ACT removal after 120 min of reaction, regardless of the acid (HCl or HNO_3) used in their synthesis.

On the other hand, Ag-doped WO_3 showed a largely improved ACT decomposition, particularly the samples synthesized with 5% content, which promoted the highest ACT degradation rates among all catalysts tested. This behavior can be explained by the existence of a greater number of Ag^+ ions available during the synthesis of the catalysts, leading to a combination of effects, among which the insertion of energy levels within the forbidden band, decreasing the band gap energy of particles with higher silver content [37], as seen in Table 1. Furthermore, as discussed previously, metallic Ag nanoparticles may form the SPR effect on the catalyst surface, increasing its ability to absorb visible light [36]. The doped catalysts synthesized with HCl exhibited better photocatalytic performance than the samples synthesized with HNO_3. This difference may be due to the presence of AgCl in the catalyst composite. As previously shown, the doped catalysts synthesized using HCl formed AgCl clusters, which can interact with $Ag@WO_3$ particles, significantly enhancing photo-generated charge-carrier separation and, consequently, photocatalytic activity. It is important to emphasize that this result was not achieved with the catalysts synthesized with HNO_3, i.e., without the formation of AgCl particles. A more in-depth discussion of the degradation

mechanism and role of AgCl will be discussed later in Section 3.8. The best result was achieved with the WO_3-5% (HCl 1.5) catalyst, which degraded 76.8% of ACT after 120 min of reaction, following a kinetic behaviour consistent with a pseudo first-order model, with a rate constant of 0.0262 min^{-1}. The degradation percentage achieved by all photocatalysts, along with the corresponding specific pseudo first-order degradation rates (*k*), are summarized in Table 2. These results clearly show that the experimental data were well fitted to pseudo first-order kinetics, with the doped photocatalysts exhibiting considerable enhancement of the ACT degradation rates compared to the pure materials.

In order to evaluate the influence of the calcination process, the WO_3-5% (HCl 1.5) catalyst was calcinated at 200 °C for 2 h, and used in an additional degradation experiment for comparing with the non-calcined sample. The assay resulted in 77.3% degradation of ACT after 120 min of reaction, equivalent to a pseudo first-order kinetic constant of 0.0422 min^{-1}. No significant difference in the photocatalytic efficiency was thus observed between calcined and non-calcined samples, indicating that there is no need for thermal treatment following the synthesis procedure, therefore reducing its costs.

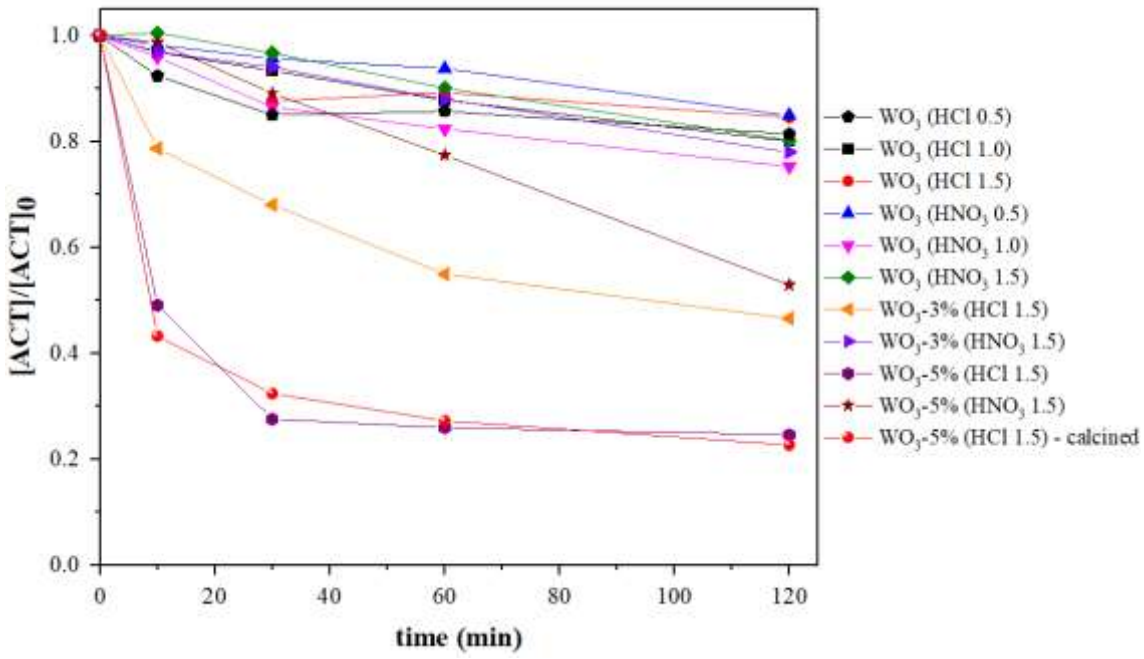

Fig. 7. Photocatalytic performance of pure and doped WO_3 photocatalysts in the degradation of acetaminophen ($[ACT]_0$ = 5.03 ± 0.09 mg L^{-1}) under simulated sunlight.

Catalyst	ACT degradation (%)[1]	k (min^{-1})[2]	R^2
WO_3 (HCl 0.5)	18.6	0.0057	0.983
WO_3 (HCl 1.0)	19.9	0.0024	0.986
WO_3 (HCl 1.5)	15.4	0.0015	0.982
WO_3 (HNO_3 0.5)	15.1	0.0013	0.992
WO_3 (HNO_3 1.0)	24.7	0.0048	0.998
WO_3 (HNO_3 1.5)	19.8	0.0018	0.993
WO_3-3% (HCl 1.5)	53.3	0.0105	0.988
WO_3-3% (HNO_3 1.5)	24.3	0.0024	0.991
WO_3-5% (HCl 1.5)	75.4	0.0458	0.967
WO_3-5% (HNO_3 1.5)	47.1	0.0050	0.991
WO_3-5% (HCl 1.5) - calcined	77.3	0.0422	0.902

[1]After 120 min of reaction; [2]Calculated in the first 30 min of reaction.

Table 2. ACT degradation rates and pseudo first-order kinetic constants for pure and doped WO_3 catalysts.

The stability of the WO_3-5% (HCl 1.5) catalyst for ACT degradation was evaluated by reuse tests, which lasted 120 min, and were performed according to the photocatalytic experiments described in Section 2.4, starting with six runs. After each cycle, the photocatalysts were washed by resuspension and centrifugation for three times with ethanol and once with water, then dried at 80 °C for 24 h, and reused in the next run. For each run, the washed and dried photocatalysts were mixed to get a total of 10 mg. As seen in Figure 8a, a small decrease in the photocatalytic activity was found, thus confirming the photocatalytic material.

The XRD patterns of the fresh and used photocatalysts over four cycles are shown in Figure 8b, and indicate that most of the peaks remain the same, except by an extra diffraction peak that appeared in the used catalyst. This peak, at $2\theta = 38.1°$, is indexed to the (111) plane of cubic Ag (JCPDS Card No. 00-004-0783), indicating that Ag^+ ions from AgCl were photo-reduced during the photocatalytic experiments [38]. It is known that an adequate Ag^0/Ag^+ ratio is crucial for effective charge separation, playing an important role in the photocatalytic process. However, if this ratio is high, a silver cluster can be formed, becoming a charge-recombination center for the photogenerated carriers, hindering the photocatalytic activity [5].

Based on this, the small decrease in photocatalytic activity after four cycles can be explained by an increase in the Ag^0/Ag^+ ratio or also by the moderately soluble nature of the Ag^+ ions in the aqueous medium [5]. The XRD peaks confirm the chemical stability of the photocatalyst, a characteristic also noticed by Yu et al. [3], who reported that the comparatively high stability of doped WO_3 photocatalysts is maintained, since the XRD patterns from fresh and reacted samples are similar after four runs.

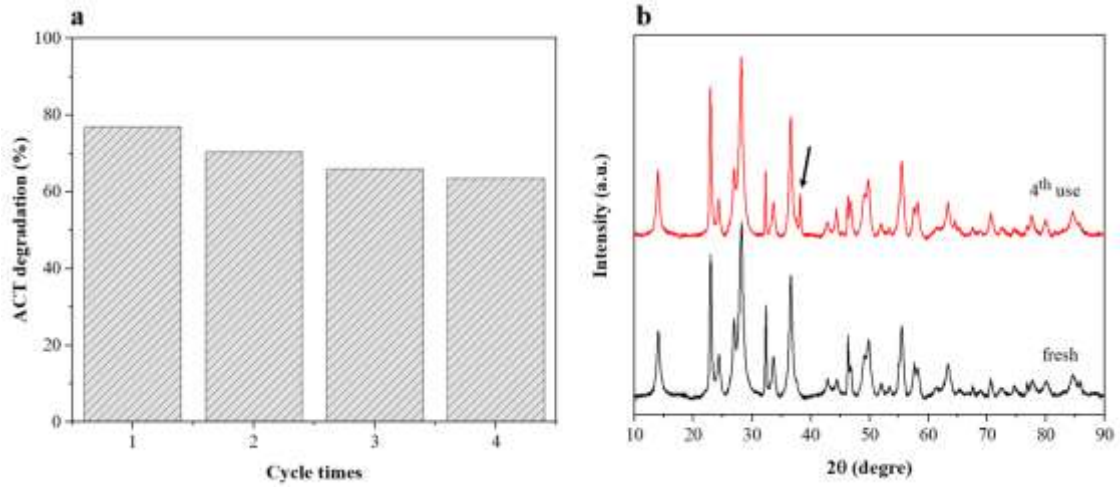

Fig. 8. (a) Reuse tests of the WO_3-5% (HCl 1.5), after 120 min; (b) XRD diffraction peaks of the fresh catalyst and after the 4th cycle of use.

3.6. Study of ACT degradation kinetics

For the evaluation of degradation kinetics, photocatalytic assays were performed with the WO_3-5% (HCl 1.5) material, which showed the best degradation performance, varying the initial ACT concentrations. Figures 9a-b allow observing that the increase in the initial ACT concentration led to a decrease in the degradation efficiency. This result is expected, since an increase in the concentration of ACT molecules requires a proportional amount of $^{\bullet}OH$ and $O_2^{\bullet-}$ radicals formed on the semiconductor surface in order to be oxidized. The generation rate and steady-state concentration of these species, however, remained the same, since fixed experimental conditions were used. As a result, the degradation efficiency decreased [39]. In addition, the photocatalyst might have been deactivated by the intermediate by-products formed from ACT degradation, which may be adsorbed onto the active sites and diffused from them at slower rates [39].

The Langmuir-Hinshelwood (L-H) expression was successfully (Figure 9c) applied to model the photocatalytic degradation of ACT for the WO_3-5% (HCl 1.5) catalyst. The data were fitted to the linearized L-H model (Equation 1), where k (min^{-1}) is the pseudo first-order specific degradation rate, k_{int} (mg L^{-1} min^{-}

^{1}) is the intrinsic reaction rate constant, and K_{ACT} (L mg^{-1}) corresponds to the ACT adsorption constant onto the catalyst surface in the aqueous suspension. It is worth observing that the L-H equation can be approximated to the pseudo first-order kinetics when $K_{ACT} \times C_0 << 1$ [40]. A satisfactory linear correlation was achieved ($R^2 = 0.955$), with $k_{int} = 0.288$ mg L^{-1} min^{-1} and $K_{ACT} = 0.113$ L mg^{-1}. It is important to mention that so far, degradation kinetic studies using WO_3-based photocatalysts have been limited to a few papers [41,42].

$$\frac{1}{k} = \frac{1}{k_{int}}[ACT]_0 + \frac{1}{k_{int}\,K_{ACT}} \quad (1)$$

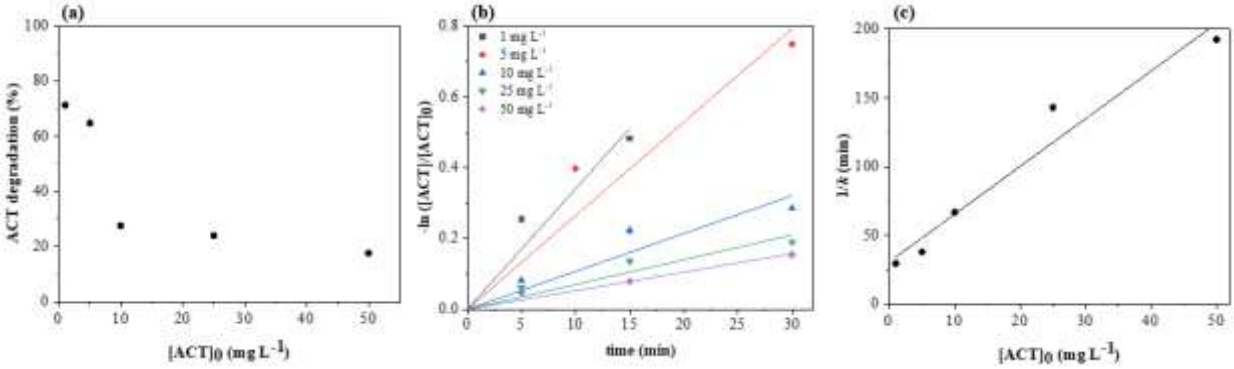

Fig. 9. (a) ACT degradation at various initial concentrations; (b) pseudo first-order kinetics; and (c) linearized L-H kinetics. All the experiments conducted using the WO_3-5% (HCl 1.5) catalyst.

3.7. Role of oxidizing species

During the photocatalytic degradation process, high reactive oxidizing species are generated from the interaction of adsorbed molecules with active holes and electron pairs generated on the irradiated semiconductor surface, which are essential for understanding the photocatalysis mechanism [43]. Among these species, it has been reported that superoxide radical anions ($O_2^{\bullet-}$) and hydroxyl radicals ($^{\bullet}OH$), besides the holes (h^+) themselves, are the main active [44]. Hence, additional experiments were performed to explore the effect of these species. For this, isopropanol, potassium iodine (KI), and 1,4-hydroquinone at 0.02 mol L^{-1} initial concentration each were selected as $^{\bullet}OH$, h^+, and $O_2^{\bullet-}$ scavengers, respectively [43,45]. All the experiments lasted 60 min, and were performed using 10 mg of WO_3-5% (HCl 1.5) catalyst, 10 mL of ACT solution at 5 mg L^{-1} of initial concentration. So far, the effect of oxidizing species using WO_3-based photocatalysts has been explored by just a few works [46,47].

As shown in Figure 10, when 1,4-hydroquinone was added to the reaction system, the photocatalytic degradation was completely suppressed, with the ultimate ACT percent removal plummeting from 64.8% in the absence of scavengers to 0%. This result suggests that $O_2^{\bullet-}$ radical anions were the major reactive

species in the photocatalytic degradation of ACT with the WO_3-based photocatalyst. When isopropanol was added to the system, the photocatalytic efficiency also suffered some suppression, with the ACT % removal after 60 min decreasing to 43.4%, which indicates that •OH radicals play an important role as well, but are not the main radicals involved in the photodegradation process.

Surprisingly though, when KI was added to the system, it accelerated ACT degradation, leading to an ultimate 92.7% ACT removal. A possible explanation for this result could be that the h^+ scavenging effect of KI helped inhibiting charge recombination to some extent. Thus, surface-trapped electrons could participate in the degradation mechanism by contributing to the formation of other reactive species, or directly in the O_2 reduction reaction (Equation 2) [48] leading to the generation of $O_2^{\bullet-}$ radicals, the major reactive species involved in ACT degradation. Finally, an extra experiment was conducted in which methanol was used to quench h^+ [49]. In that case, Figure 10 indicates that no significant difference in ACT degradation was observed in comparison with the experiment performed in the absence of scavengers, suggesting that h^+ may not be relevant in the photocatalytic ACT degradation using the WO_3-5% (HCl 1.5) catalyst.

$$O_2 + e^- \rightarrow O_2^{\bullet-} \quad (2)$$

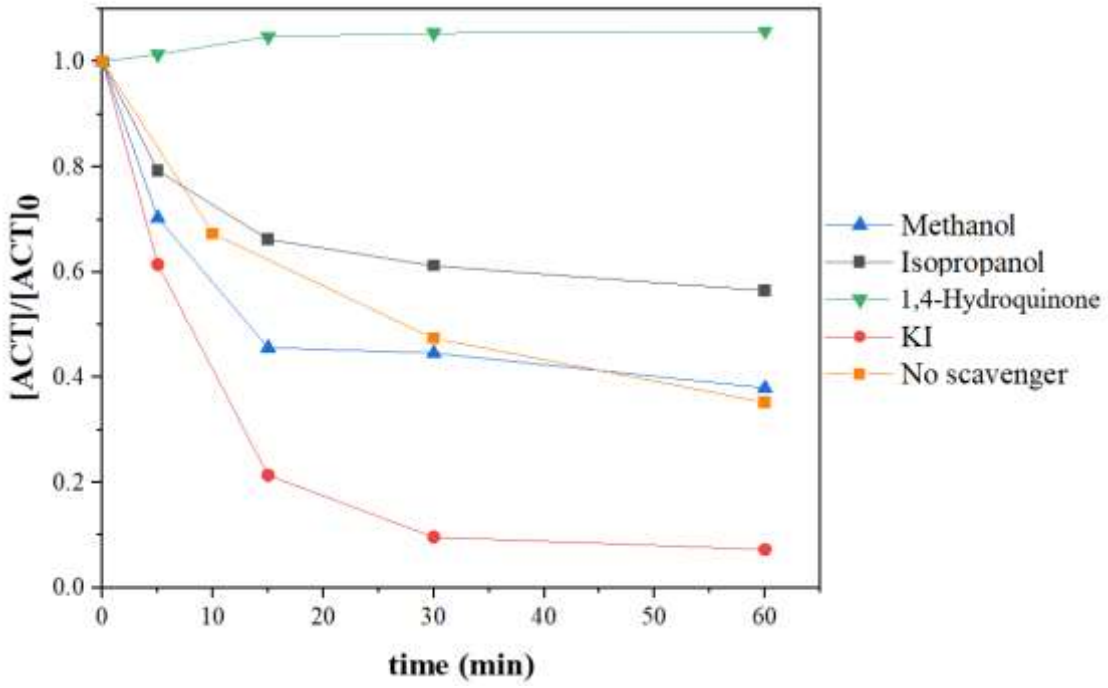

Fig. 10. Effect of different radical scavengers on the efficiency of ACT degradation using WO_3-5% (HCl 1.5) catalyst. Conditions: $[ACT]_0$ = 5.02 ± 0.12 mg L^{-1}; $m_{catalyst}$ = 10 mg; $V_{solution}$ = 10 mL; dosage of scavengers = 0.02 mol L^{-1}; irradiation time = 60 min.

3.8. Photodegradation mechanism

A discussion of the degradation mechanism is presented for the WO_3-5% (HCl 1.5) catalyst, which resulted in the best ACT degradation. The valance and conduction bands of WO_3 and AgCl were calculated through Equations 3 and 4, in which E_{VB}, E_{CB}, and E_g refer to the potential of the valence and conduction bands, and the band gap energy, respectively; E^e denotes the energy of the free electron (~4.5 eV), while χ corresponds to the electronegativity of the materials, i.e., 6.59 and 6.08 eV for WO_3 and AgCl, respectively [25].

$$E_{VB} = \chi - E^e + 0.5E_g \quad (3)$$

$$E_{CB} = E_{VB} - E_g \quad (4)$$

The VB and CB values for pure WO_3 synthesized using HCl 1.5 were found to be 3.41 and 0.77 eV, respectively. The band values for AgCl were selected from literature, equal to 3.08 eV for VB and 0.07 eV for CB [25]. Thus, according to the band positions and the results mentioned so far, a possible mechanism for the degradation of ACT over the WO_3-5% (HCl 1.5) composite is proposed (Figure 11). In accordance with the band gap energies, it is known that WO_3 (2.64 eV - Table 1) can be excited by visible light, while AgCl (3.01 eV [3]) cannot; however, as a solar simulator was used in our photocatalytic experiments, AgCl may be excited by the UV portion of the spectrum [32]. Accordingly, AgCl and WO_3 are excited to generate e^-/h^+ pairs. As can be seen in the TEM images (Figure 5), metallic silver was adhered to the surface of WO_3, and thus Ag particles may form the SPR effect on the WO_3 surface, enhancing its ability to absorb visible light [36]. In fact, the literature reports that WO_3 is an effective LSPR host, which is associated with the ability of its d valence-electrons to synergistically interact with silver [50]. Because the CB of AgCl is more negative than the CB of WO_3, and the VB of WO_3 is more positive than that of AgCl, the photoexcited electrons in the AgCl conduction band can quickly transfer to the CB of WO_3. At the same time, the photo-generated holes in the VB of WO_3 can migrate to the AgCl valence band. Consequently, the photo-generated e^-/h^+ pairs can be successfully separated in the WO_3-5% (HCl 1.5) AgCl/WO_3-Ag composite.

The holes accumulated in the VB of AgCl can combine with H_2O ($H_2O/^{\bullet}OH$: 2.72 eV vs. NHE) or OH^- ($OH^-/^{\bullet}OH$: 2.40 eV vs. NHE) to form $^{\bullet}OH$ radicals, which play an important role in the photocatalytic ACT degradation [51]. Meanwhile, the electrons accumulated in the CB of WO_3 cannot combine with O_2 to form $O_2^{\bullet-}$, as this band potential is more positive than the standard potential of $O_2^{\bullet-}$ ($O_2/O_2^{\bullet-}$: −0.33 eV vs. NHE) [32,51]. Likewise, even the electrons that may be in the CB of AgCl cannot combine with O_2. However, it was proven by the experiments with radical scavengers that $O_2^{\bullet-}$ radicals are the most important reactive

447 species in ACT degradation. Under these circumstances, we speculate the formation of W^{5+} and W^{6+} on the
448 photocatalyst surface during the reaction. The hexagonal phase of WO_3 as found in this work can stimulate
449 the transfer of electrons in the conduction band of semiconductor materials through the circulatory system
450 between W^{5+} and W^{6+}, and as a consequence, convert these electrons into active species, increasing the
451 activity of the photocatalyst [32]. Low-valence tungsten in the material can be excited by visible light, and
452 high-valence tungsten is generated by loss of electrons [32]. Given that, Chai et al. [32] hypothesize that
453 the W^{5+} and W^{6+} may be related to the generation of $O_2^{\bullet-}$ radicals, considering that the electrons in the CB
454 of WO_3 reduce W^{6+} to W^{5+}. Then, the electrons that were generated by the excitation of W^{5+} have enough
455 energy to reduce O_2 and thus produce $O_2^{\bullet-}$.

456 In addition, the XRD diffractogram of the used catalyst (Figure 8b) confirms the formation of metallic
457 Ag during the degradation process. Because of this, the generation of Ag^0 is proposed in Figure 11, which
458 can form the LSPR effect on the AgCl surface, contributing to its ability to absorb visible light. Finally, the
459 composite made of AgCl and WO_3-Ag may have formed an efficient heterojunction, where the active
460 species $O_2^{\bullet-}$ and $^{\bullet}OH$ contribute to delaying charge-carrier recombination and increasing the photocatalytic
461 activity of the synthesized material, comparing to bare WO_3. This mechanism is useful to understand why
462 the doped catalyst synthesized with HCl leads to greater photocatalytic activity than those prepared with
463 HNO_3. Particularly, AgCl particles and the interactions they can promote in the photocatalyst are
464 fundamental for its performance, which may not be achieved with catalysts doped only with metallic Ag
465 (i.e., synthesized with HNO_3).
466

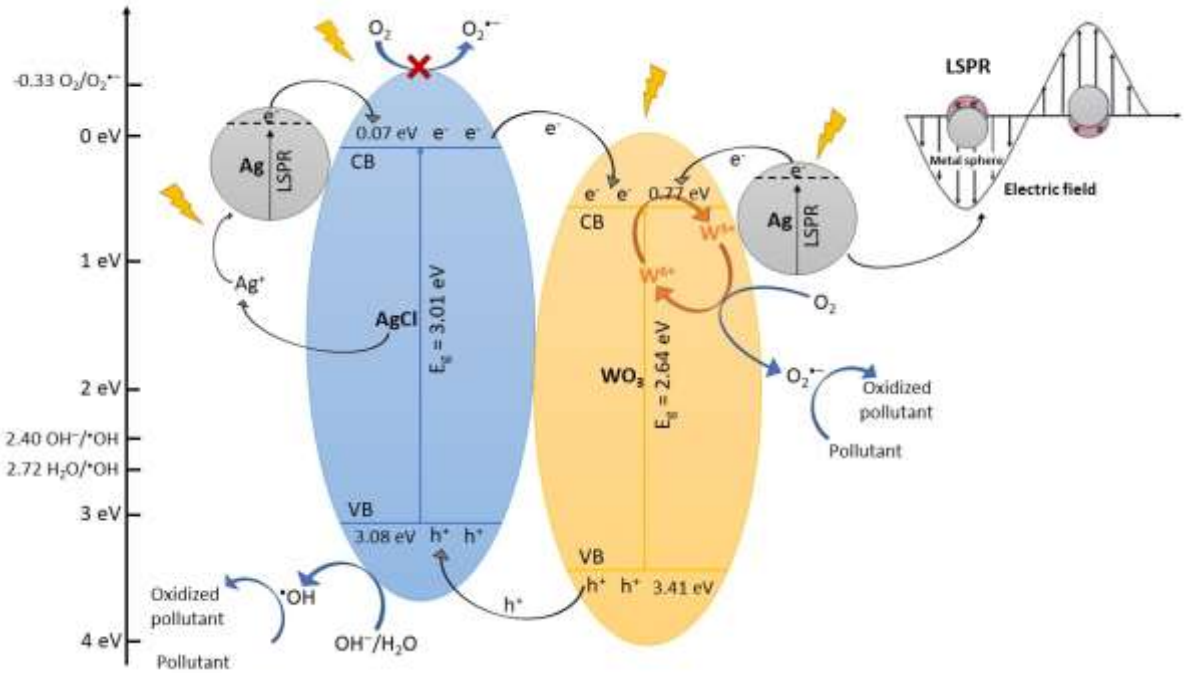

Fig. 11. Proposed photodegradation mechanism diagram of WO_3-5% (HCl 1.5) composite on the degradation of ACT under simulated sunlight irradiation.

4. Conclusions

In this work, pure and doped WO_3 photocatalysts were successfully synthetized by a facile one-step hydrothermal method, in which the particular effects of HCl or HNO_3 in the synthesis process were evaluated for the first time. For the pure WO_3 materials, HCl or HNO_3 did not lead to significant differences regarding morphology or photocatalytic activity.

However, doped catalysts produced using HCl resulted in particles of well uniform flower-like morphology, with higher uniformity compared to those produced using HNO_3. Furthermore, when HCl was used, the catalysts resulted in a composite containing WO_3, Ag and AgCl, while when HNO_3 was used, only Ag was the dopant. Yet, Ag played an important role in improving the degradation efficiency because of the LSPR effect.

The photocatalytic activity was markedly enhanced with the incorporation of AgCl and Ag to WO_3, resulting in maximum acetaminophen degradation of 76.8% after 120 min with the WO_3-5% (HCl 1.5) catalyst under simulated sunlight. Thus, this composite The Langmuir-Hinshelwood (L-H) kinetic expression was successfully applied for this catalyst, resulting k_{int} = 0.288 mg L^{-1} min^{-1} and K_{ACT} = 0.113 L mg^{-1}.

The stability evaluation showed that the synthesized materials were stable over four cycle runs, with no significant decrease in the degradation efficiency. Finally, the role of oxidizing species, evaluated by using different active species scavengers, revealed that $O_2^{\bullet-}$ radical anions were the major reactive species in the photocatalytic degradation of ACT with the WO_3-5% (HCl 1.5) photocatalyst. In this context, the formation of W^{5+} and W^{6+} on the photocatalyst surface was speculated to be related to the generation of $O_2^{\bullet-}$ radicals.

Acknowledgements

The authors express their gratitude to the São Paulo Research Foundation (FAPESP, grant no. 2018/21271-6), to the Brazilian National Council for Scientific and Technological Development (CNPq, grant no.131467/2017-4) and to the Coordination for the Improvement of Higher Education Personnel – Brazil (CAPES) – Finance Code 001. The authors are also thankful to the Multiuser Central Facilities (UFABC), to the Electrochemistry and Corrosion Laboratory (ChE Department, USP), to the Laboratory for Technological Characterization - LCT (Mining and Petroleum Eng. Department, USP), to LapCat (ChE Department, USP) and to F. de J. Trindade for the support with materials characterization.

References

[1] H. Zheng, J.Z. Ou, M.S. Strano, R.B. Kaner, A. Mitchell, K. Kalantar-Zadeh, Nanostructured tungsten oxide - Properties, synthesis, and applications, Adv. Funct. Mater. 21 (2011) 2175–2196. https://doi.org/10.1002/adfm.201002477.

[2] M.A. Suliman, M.A. Gondal, M.A. Dastageer, G.K. Chuah, C. Basheer, Method for visible light-induced photocatalytic degradation of methylparaben in water using nanostructured Ag/AgBr@m-WO_3, Photochem. Photobiol. 95 (2019) 1485–1494. https://doi.org/10.1111/php.13118.

[3] C. Yu, F. Chen, Z. Liu, K. Yang, H. Ji, D. Li, W. Xie, S. Li, Facile synthesis of a robust visible-light-driven AgCl/WO_3 composite microrod photocatalyst, J. Alloys Compd. 809 (2019) 151844–151854. https://doi.org/10.1016/j.jallcom.2019.151844.

[4] H. Liu, C. Niu, H. Guo, C. Liang, D. Huang, L. Zhang, Y. Yang, L. Li, In suit constructing 2D/1D $MgIn_2S_4$/CdS heterojunction system with enhanced photocatalytic activity towards treatment of wastewater and H_2 production, J. Colloid Interface Sci. 576 (2020) 264–279. https://doi.org/10.1016/j.jcis.2020.05.025.

[5] S. Adhikari, D. Sarkar, High efficient electrochromic WO_3 nanofibers, Electrochim. Acta. 138 (2014) 115–123. https://doi.org/10.1016/j.electacta.2014.06.062.

[6] J.C. Murillo-Sierra, A. Hernández-Ramírez, L. Hinojosa-Reyes, J.L. Guzmán-Mar, A review on the development of visible light-responsive WO_3-based photocatalysts for environmental applications, Chem. Eng. J. Adv. 5 (2021) 100070–100091. https://doi.org/10.1016/j.ceja.2020.100070.

[7] W. Mu, X. Xie, X. Li, R. Zhang, Q. Yu, K. Lv, H. Wei, Y. Jian, Characterizations of Nb-doped WO_3 nanomaterials and their enhanced photocatalytic performance, RSC Adv. 4 (2014) 36064–36070. https://doi.org/10.1039/C4RA04080E.

[8] B. Ahmed, S. Kumar, A.K. Ojha, P. Donfack, A. Materny, Facile and controlled synthesis of aligned WO_3 nanorods and nanosheets as an efficient photocatalyst material, Spectrochim. Acta Part A Mol. Biomol. Spectrosc. 175 (2017) 250–261. https://doi.org/10.1016/j.saa.2016.11.044.

[9] S.K. Biswas, J.-O. Baeg, S.-J. Moon, K.-J. Kong, W.-W. So, Morphologically different WO_3 nanocrystals in photoelectrochemical water oxidation, J. Nanoparticle Res. 14 (2012) 667–679. https://doi.org/10.1007/s11051-011-0667-6.

[10] J. Yu, L. Qi, B. Cheng, X. Zhao, Effect of calcination temperatures on microstructures and photocatalytic activity of tungsten trioxide hollow microspheres, J. Hazard. Mater. 160 (2008) 621–628. https://doi.org/10.1016/j.jhazmat.2008.03.047.

[11] M.A.M. Khan, S. Kumar, T. Ahamad, A.N. Alhazaa, Enhancement of photocatalytic and electrochemical properties of hydrothermally synthesized WO_3 nanoparticles via Ag loading, J. Alloys Compd. 743 (2018) 485–493. https://doi.org/10.1016/j.jallcom.2018.01.343.

[12] Y.-H. Xiao, C.-Q. Xu, W.-D. Zhang, Facile synthesis of Ni-doped WO_3 nanoplate arrays for effective photoelectrochemical water spliting, J. Solid State Electrochem. 21 (2017) 3355–3364. https://doi.org/https://doi.org/10.1007/s10008-017-3680-6.

[13] V. Rajendran, B. Deepa, Studies on the structural, morphological, optical, electro chemical and antimicrobial activity of bare, Cu and Ag @ WO_3 nanoplates by hydrothermal method, J. Inorg. Organimetallic Polym. Mater. 28 (2018) 1574–1586. https://doi.org/10.1007/s10904-018-0846-3.

[14] H. Zhang, D. Yu, W. Wang, P. Gao, K. Bu, L. Zhang, S. Zhong, B. Liu, Multiple heterojunction system of $Bi_2MoO_6/WO_3/Ag_3PO_4$ with enhanced visible-light photocatalytic performance towards dye degradation, Adv. Powder Technol. 30 (2019) 1910–1919.

https://doi.org/https://doi.org/10.1016/j.apt.2019.06.010.

[15] X. Zhao, X. Zhang, D. Han, L. Niu, Ag supported Z-scheme $WO_{2.9}$/g-C_3N_4 composite photocatalyst for photocatalytic degradation under visible light, Appl. Surf. Sci. 501 (2020) 144258–144267. https://doi.org/10.1016/j.apsusc.2019.144258.

[16] P. Jineesh, T.C. Bhagya, R. Remya, S.M.A. Shibli, Photocatalytic hydrogen generation by WO_3 in synergism with hematite-anatase heterojunction, Int. J. Hydrogen Energy. 45 (2020) 18946–18960. https://doi.org/10.1016/j.ijhydene.2020.05.043.

[17] Y. Yang, X. Zhang, C. Niu, H. Feng, P. Qin, H. Guo, C. Liang, L. Zhang, H. Liu, L. Li, Dual-channel charges transfer strategy with synergistic effect of Z-scheme heterojunction and LSPR effect for enhanced quasi-full-spectrum photocatalytic bacterial inactivation: new insight into interfacial charge transfer and molecular oxygen activation, Appl. Catal. B Environ. 264 (2020) 118465–118480. https://doi.org/10.1016/j.apcatb.2019.118465.

[18] X. Liu, J. Hu, J. Li, Y. Hu, Y. Shao, H. Yang, G. Tong, H. Qian, Facile synthesis of Ag_2WO_4/AgCl nanorods for excellent photocatalytic properties, Mater. Lett. 91 (2013) 129–132. https://doi.org/10.1016/j.matlet.2012.09.078.

[19] J. Li, C. Yu, C. Zheng, A. Etogo, Y. Xie, Y. Zhong, Y. Hu, Facile formation of Ag_2WO_4/AgX (X = Cl , Br, I) hybrid nanorods with enhanced visible-light-driven photoelectrochemical properties, Mater. Res. Bull. 61 (2015) 315–320. https://doi.org/10.1016/j.materresbull.2014.10.018.

[20] X. Zhao, L. Song, S. Zhang, Synthesis of AgCl/Ag_3PO_4 composite photocatalysts and study on photodegradation activity based on a continuous reactor, Photochem. Photobiol. 94 (2018) 484–490. https://doi.org/10.1111/ijlh.12426.

[21] M. Geravand, F. Jamali-sheini, Synthesis and physical properties of un- and Zn-doped Ag_2S nanoparticles, Adv. Powder Technol. 30 (2019) 347–358. https://doi.org/10.1016/j.apt.2018.11.012.

[22] S. Sousa, F. Xavier, E.A. Arau, J. Ricardo, R. Albuquerque, C. Couceiro, P. Roge, W. Ricardo, M. Elias, D. Matos, M. Rita, D.M. Chaves, Hydrothermal synthesis, structural characterization and photocatalytic properties of b-Ag_2MoO_4 microcrystals: Correlation between experimental and theoretical data, Arab. J. Chem. 13 (2020) 2806–2825. https://doi.org/10.1016/j.arabjc.2018.07.011.

[23] M. Mahjoubian, A. Sadat, M. Sheykhan, Chemosphere Toxicological effects of Ag_2O and Ag_2CO_3

doped TiO_2 nanoparticles and pure TiO_2 particles on zebra fish (*Danio rerio*), Chemosphere. 263 (2021) 128182–128196. https://doi.org/10.1016/j.chemosphere.2020.128182.

[24] L. Li, C. Niu, H. Guo, J. Wang, M. Ruan, L. Zhang, C. Liang, H.-Y. Liu, Y.-Y. Yang, Efficient degradation of Levofloxacin with magnetically separable $ZnFe_2O_4$/NCDs/Ag_2CO_3 Z-scheme heterojunction photocatalyst: Vis-NIR light response ability and mechanism insight, Chem. Eng. J. 383 (2020) 123192–123206. https://doi.org/10.1016/j.cej.2019.123192.

[25] R.A. Senthil, S. Osman, J. Pan, M. Sun, A. Khan, V. Yang, Y. Sun, A facile single-pot synthesis of WO_3/AgCl composite with enhanced photocatalytic and photoelectrochemical performance under visible-light irradiation, Colloids Surfaces A. 567 (2019) 171–183. https://doi.org/https://doi.org/10.1016/j.colsurfa.2019.01.056.

[26] N. Li, T. Chang, H. Gao, X. Gao, L. Ge, Morphology-controlled WO_{3-x} homojunction: hydrothermal synthesus, adsorption properties, and visible-light-driven photocatalytic and chromic properties., Nanotechnology. 30 (2019) 415601–415612. https://doi.org/10.1088/1361-6528/ab2a38.

[27] W. Fang, Y. Yang, H. Yu, X. Dong, T. Wang, W. Wang, Z. Liu, B. Zhao, M. Yang, One Step Synthesis of Flower-like WO_3 Nanostructures for High Sensitivity Room Temperature NOx Gas Sensor, RSC Adv. 3 (2016) 106880–106886. https://doi.org/10.1039/b000000x.

[28] M. Ahmadi, R. Younese, M.J.-F. Guinel, Synthesis of tungsten oxide nanoparticles using hydrothermal method at ambient pressure, J. Mater. Res. 29 (2014) 1424–1430. https://doi.org/10.1557/jmr.2014.155.

[29] R. Ponnusamy, A. Gangan, B. Chakraborty, C.S. Rout, Tuning the pure monoclinic phase of WO_3 and WO_3-Ag nanostructures for non-enzymatic glucose sensing application with theoretical insight from electronic structure simulations, J. Appl. Phys. 123 (2018) 024701–024710. https://doi.org/10.1063/1.5010826.

[30] B.A.D. Nandiyanto, R. Zaen, R. Oktiani, Correlation between crystallite size and photocatalytic performance of micrometer-sized monoclinic WO_3 particles, Arab. J. Chem. 13 (2020) 1283–1296. https://doi.org/10.1016/j.arabjc.2017.10.010.

[31] L. Su, L. Luo, J. Wang, T. Song, W. Tu, Z. Wang, Lamellar flower-like porous MoS_2 as an efficient cocatalyst to boost photocatalytic hydrogen evolution of CdS, Catal. Sci. Technol. 11 (2021) 1292–1297. https://doi.org/https://doi.org/10.1039/D0CY02100H.

606 [32] C. Chai, J. Liu, Y. Wang, X. Zhang, D. Duan, C. Fan, Y. Wang, Enhancement in photocatalytic
607 performance of Ag–AgCl decorated with h-WO_3 and mechanism insight, Appl. Phys. A. 125 (2019)
608 96–106. https://doi.org/10.1007/s00339-019-2384-4.
609 [33] X. Zhu, H. Xu, Y. Yao, H. Liu, J. Wang, Y. Pu, W. Feng, S. Chen, Effects of Ag^0-modification and
610 Fe^{3+}-doping on the structural, optical and photocatalytic properties of TiO_2, RSC Adv. 9 (2019)
611 40003–40012. https://doi.org/10.1039/c9ra08655b.
612 [34] Y. Ding, C. Zhao, Y. Li, Z. Ma, X. Lv, Effect of calcination temperature on the structure and
613 catalytic performance of the Cu-MCM-41 catalysts for the synthesis of dimethyl carbonate, Quim.
614 Nova. 41 (2018) 1156–1161. https://doi.org/10.21577/0100-4042.20170291.
615 [35] K.H. Leong, B.L. Gan, S. Ibrahim, P. Saravanan, Synthesis of surface plasmon resonance (SPR)
616 triggered Ag/TiO_2 photocatalyst for degradation of endocrine disturbing compounds, Appl. Surf.
617 Sci. 319 (2014) 128–135. https://doi.org/10.1016/j.apsusc.2014.06.153.
618 [36] H. Jung, I. Yeo, T. Kim, H. Ki, H. Gu, Surface plasmon resonance effect of silver nanoparticles on
619 a TiO_2 electrode for dye-sensitized solar cells, Appl. Surf. Sci. 432 (2018) 266–271.
620 https://doi.org/10.1016/j.apsusc.2017.04.237.
621 [37] S. Ramkumar, G. Rajarajan, Enhanced visible light photocatalytic activity of pristine and silver
622 (Ag) doped WO_3 nanostructured thin films, J. Mater. Sci. Mater. Electron. 27 (2016) 12185–12192.
623 https://doi.org/10.1007/s10854-016-5373-9.
624 [38] R. Qiao, M. Mao, E. Hu, Y. Zhong, J. Ning, Y. Hu, Facile formation of mesoporous
625 $BiVO_4$/Ag/AgCl heterostructured microspheres with enhanced visible-light photoactivity, Inorg.
626 Chem. 54 (2015) 9033–9039. https://doi.org/10.1021/acs.inorgchem.5b01303.
627 [39] M.J.N. Gotostos, C.C. Su, M.D.G. De Luna, M.C. Lu, Kinetic study of acetaminophen degradation
628 by visible light photocatalysis, J. Environ. Sci. Heal. - Part A Toxic/Hazardous Subst. Environ.
629 Eng. 49 (2014) 892–899. https://doi.org/10.1080/10934529.2014.894310.
630 [40] K.V. Kumar, K. Porkodi, F. Rocha, Langmuir-Hinshelwood kinetics - A theoretical study, Catal.
631 Commun. 9 (2008) 82–84. https://doi.org/10.1016/j.catcom.2007.05.019.
632 [41] C. Zhao, D. Li, Y. Liu, C. Feng, Z. Zhang, N. Sugiura, Y. Yang, Photocatalytic removal of
633 microcystin-LR by advanced WO_3-based nanoparticles under simulated solar light, Sci. World J.
634 2015 (2015). https://doi.org/10.1155/2015/720706.
635 [42] J. Rong, T. Zhang, F. Qiu, X. Rong, X. Zhu, X. Zhang, Preparation of hierarchical

micro/nanostructured Bi_2S_3-WO_3 composites for enhanced photocatalytic performance, J. Alloys Compd. 685 (2016) 812–819. https://doi.org/10.1016/j.jallcom.2016.06.210.

[43] D.B. Hernández-Uresti, D. Sanchez-Martinez, L.M. Torres-Martinez, Novel visible light-driven $PbMoO_4$/g-C_3N_4 hybrid composite with enhanced photocatalytic performance, J. Photochem. Photobiol. A Chem. 345 (2017) 21–26. https://doi.org/10.1016/j.jphotochem.2017.05.013.

[44] S. Deng, Z. Yang, G. Lv, Y. Zhu, H. Li, F. Wang, X. Zhang, WO_3 nanosheets/g-C_3N_4 nanosheets' nanocomposite as an effective photocatalyst for degradation of rhodamine B, Appl. Phys. A Mater. Sci. Process. 125 (2019) 44–55. https://doi.org/10.1007/s00339-018-2331-9.

[45] O. Fónagy, E. Szabó-Bárdos, O. Horváth, 1,4-Benzoquinone and 1,4-hydroquinone based determination of electron and superoxide radical formed in heterogeneous photocatalytic systems, J. Photochem. Photobiol. A Chem. 407 (2021) 113057–113071. https://doi.org/10.1016/j.jphotochem.2020.113057.

[46] D. Zhang, J. Wang, In situ photoactivated plasmonic Ag_3PO_4@silver as a stable catalyst with enhanced photocatalytic activity under visible light, Mater. Res. 20 (2017) 702–711. https://doi.org/10.1590/1980-5373-MR-2016-0800.

[47] D. Costenaro, C. Bisio, F. Carniato, A.M. Katsev, S.L. Safronyuk, N. Starodub, C. Tiozzo, M. Guidotti, Tungsten oxide: a catalyst worth studying for the abatement and decontamination of chemical warfare agents, Glob. Secur. Heal. Sci. Policy. 2 (2017) 62–75. https://doi.org/10.1080/23779497.2017.1330662.

[48] J. Low, C. Jiang, B. Cheng, S. Wageh, A.A. Al-Ghamdi, J. Yu, A Review of Direct Z-Scheme Photocatalysts, Small Methods. 1 (2017) 1700080–1700101. https://doi.org/10.1002/smtd.201700080.

[49] M. Shen, M.A. Henderson, Identification of the active species in photochemical hole scavenging reactions of methanol on TiO_2, J. Phys. Chem. Lett. 2 (2011) 2707–2710. https://doi.org/10.1021/jz201242k.

[50] Y. Yao, F. Ji, M. Yin, X. Ren, Q. Ma, J. Yan, S.F. Liu, Ag nanoparticle-sensitized WO_3 hollow nanosphere for localized surface plasmon enhanced gas sensors, ACS Appl. Mater. Interfaces. 8 (2016) 18165–18172. https://doi.org/10.1021/acsami.6b04692.

[51] X. Yuan, L. Jiang, X. Chen, L. Leng, H. Wang, Z. Wu, T. Xiong, J. Liang, G. Zeng, Highly efficient visible-light-induced photoactivity of Z-scheme Ag_2CO_3/Ag/WO_3 photocatalysts for organic

pollutant degradation, Environ. Sci. Nano. 4 (2017) 2175–2185. https://doi.org/10.1039/C7EN00713B.